Bulk Separation of Multicomponent Gas Mixtures by Pressure Swing Adsorption: Pore/Surface Diffusion and Equilibrium Models

A theoretical and experimental study is performed for the bulk separation of a ternary mixture by pressure swing adsorption. Three concentrated products can be obtained by cycling the pressure in the adsorber. Three models are formulated for the cyclic process: equilibrium, Knudsen diffusion, and Knudsen plus surface diffusion. The latter model provides the best results when compared with the experimental data, due to the important contribution of surface flux to the total flux in the sorbent pores.

S.-J. Doong and R. T. Yang
Department of Chemical Engineering
State University of New York
Buffalo, NY 14260

SCOPE

An increasing number of commercial applications are being discovered for pressure swing adsorption (PSA) because of its low energy requirements and costs. The applications are, however, somewhat limited to gas purification processes, with the only bulk separation being for O_2 or N_2 from air. Multicomponent bulk separation by PSA using one sorbent and a single PSA unit, despite its promising commercial value, has not appeared in the literature. In this study, an $H_2/CH_4/CO_2$ mixture (one-third each by volume) is separated by PSA using activated carbon and involving five basic cyclic steps: I repressurization, II adsorption, III cocurrent depressurization, IV countercurrent blowdown, and V purge. Following the order of increasing adsorption strength, H_2 is produced in step II and in the early stage of step III. The later cut in step III yields CH_4, and steps IV and V produce CO_2. A basic understanding of the cyclic process is obtained by modeling. Three models are formulated and compared with experimental results: equilibrium model, Knudsen diffusion model, and Knudsen plus surface diffusion model.

CONCLUSIONS AND SIGNIFICANCE

Bulk separation of the ternary mixture $H_2/CH_4/CO_2$ is accomplished by PSA using a single sorbent. High-purity products of H_2 and CH_4 are obtained, whereas the product purity for CO_2 only reaches 60% due to the low selectivity between CO_2/CH_4 on activated carbon. Of the three models for the cyclic process, the Knudsen plus surface diffusion model provides the best results when compared to the experimental data. Due to the high surface coverage, surface diffusion significantly contributes to the total flux in the sorbent pores, generally over 50% in the PSA process. Accounting for the strong dependence of surface diffusivity on surface coverage, the effects of purge/feed ratio, pressure ratio, feed rate, and end pressure of depressurization on the separation are predictable by the model. A basic understanding of the bed dynamics also is presented.

Introduction

Pressure swing adsorption (PSA) is a gas separation process in which the adsorbent is regenerated by reducing the partial pressure of the adsorbed component. Partial pressure reduction can be accomplished rather rapidly by lowering the total pressure or using a purge gas. Since its invention by Skarstrom (1959), originally proposed for air drying using a simple two-column scheme, an increasing number of commercial applications have recently been found that demand low energy inputs. Recent reviews of the process have been made by Keller (1983), Cassidy and Holmes (1984), and Ruthven (1984).

Most of the commercial PSA processes are used for gas purification, the desired products being the weakly adsorbed components, and only one product is obtained. Bulk separation of a binary mixture (50/50 mixture of H_2/CH_4) giving two products has been studied by Yang and Doong (1985), who also provide a literature review of the PSA processes for bulk separations. Limited information exists in the literature on PSA separations of multicomponent mixtures that give as many products. Nataraj and Wankat (1982) proposed two schemes for fractionation of a mixture containing N solutes and a carrier gas requiring $N + 1$ columns. Knaebel (1984), and Wankat and Tondeur (1984) proposed similar PSA processes using sorbents with complementary selectivities contained in separate columns. However, no experimental results have been available for these processes. Sircar (1979) invented a PSA process using two batteries of columns containing two sorbents which gave two high-purity products from a three-component mixture. In the present work, a one-column, one-sorbent PSA process was studied for the bulk separation of a ternary mixture (multicolumn arrangements can be made, as in conventional PSA processes).

Despite the wide commercial application of PSA, its theoretical understanding remains in a primitive stage. Most of the PSA models are based on the simplest equilibrium theory, which includes models by: Shendalman and Mitchell (1972), Weaver and Hamrin (1974), Fernandez and Kenney (1983), Chan et al. (1981), Cheng and Hill (1983), Nataraj and Wankat (1982) for PSA, and by Turnock and Kadlec (1971) for a single-column PSA process. For the air-drying PSA process, the models by Chihara and Suzuki (1983), and Carter and Wyszynski (1983) have accounted for the mass transfer rates in porous sorbent by using the linear driving force approximation. All of these models with the exceptions of Turnock/Kadlec and Fernandez/Kenney deal with dilute mixtures; hence linear isotherms are used. The important features of bulk gas separation, in contrast to dilute systems, are the nonlinearity of the adsorption isotherms, the variation of gas velocity in the column, and the large temperature excursions during each cycle, all of which increase the complexity of the model. These features are included in a pore diffusion model that adequately predicts the performance of PSA for the bulk separation of binary mixtures (Yang and Doong, 1985). In this study the model has been extended to a ternary system. More noteworthy, the importance of surface diffusion accompanying a high surface coverage, which is prevalent in PSA processes, is recognized. The model proposed in this work includes the surface diffusion flux.

Description of the Process

The gas mixture to be separated contained three components: H_2, CH_4, and CO_2 at one-third each by volume. The PSA process cycle, as illustrated in Figure 1, comprised five basic steps all of which are commercially practiced. The cycle was designed to recover three products from the ternary mixture feed using a single column with one sorbent. The steps in a PSA cycle were:

I. H_2 pressurization
II. Feed or adsorption at high pressure
III. Cocurrent depressurization
IV. Countercurrent blowdown
V. H_2 purge

Step III was subdivided into IIIa and IIIb whereby two product cuts, H_2 and CH_4, respectively, were recovered.

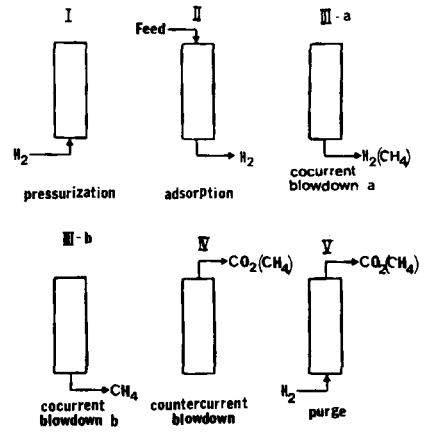

Figure 1. Cycle sequence in PSA for ternary gas separation.

In step I the bed was pressurized to the feed pressure by H_2. Gases other than pure H_2 have also been used in this step, such as the feed mixture (Yang and Doong, 1985) and the H_2 product derived from the process (Cen and Yang, 1985). The product purities were lowered but not substantially. The effluent in step II was a high-purity H_2 product. Step IIIa was used to recover the remaining H_2 in the bed (mostly in the clean portion of the bed), and in the meantime to desorb CH_4 and CO_2 in the upper portion of the bed (which were readsorbed in the lower portion). The function and the importance of this step has been discussed by Yang and Doong (1985). The effluent from further depressurization, step IIIb, yielded a high-purity CH_4 product. This step continued until CO_2 breakthrough. Steps IV and V, both operated countercurrent to the feed direction, produced a CO_2 product and provided a clean bed for the next cycle.

Two or more interconnected beds may be operated in phase so continuous feed and products are possible. However, since all beds display identical behavior, only one bed was used in the experiments.

Mathematical Models

The following simplifying assumptions are made; they have all been justified in our previous studies: ideal gas behavior, negligible axial dispersion and pressure gradient in the bed, negligible radial gradients in temperature and concentrations, and thermal equilibrium between fluid and particles. Furthermore, the transport (diffusivities) and physical (Cp, ρ) properties are assumed to be independent of temperature, since the process operates in a rather narrow temperature range.

Mass balances for the n adsorbates give:

$$\alpha \frac{\partial C_i}{\partial t} + \frac{\partial u C_i}{\partial z} - S_i = 0 \quad i = 1, 2, \ldots n \tag{1}$$

Applying ideal gas law, $C_i = Py_i/RT$, and noting $\Sigma y_i = 1$, the n equations are rewritten into an overall mass balance, Eq. 2, and $n-1$ component equations:

$$\frac{\alpha}{RT}\frac{\partial P}{\partial t} - \frac{\alpha P}{RT^2}\frac{\partial T}{\partial t} + \frac{P}{RT}\frac{\partial u}{\partial z} - \frac{uP}{RT^2}\frac{\partial T}{\partial z} - \sum_{j=1}^{n} S_j = 0 \tag{2}$$

$$\frac{\alpha P}{RT}\frac{\partial y_i}{\partial t} + \frac{uP}{RT}\frac{\partial y_i}{\partial z} + y_i \sum_{j=1}^{n} S_j - S_i = 0$$

$$i = 1, 2, \ldots n-1 \tag{3}$$

Equilibrium model

Various models arise depending on the expression for the sorption rate terms, S_i. In the simplest model, the equilibrium model, instantaneous equilibrium is assumed between the bulk flow and the adsorbed phase. Thus, S_i is replaced by $-\rho_B \partial q_i/\partial t$, where q_i is the equilibrium amount adsorbed, in equilibrium with the bulk flow concentrations. The expression for $\partial q_i/\partial t$ is:

$$\frac{\partial q_i}{\partial t} = \frac{\partial q_i}{\partial P}\frac{\partial P}{\partial t} + \frac{\partial q_i}{\partial T}\frac{\partial T}{\partial t} + \sum_{j=1}^{n-1} \frac{\partial q_i}{\partial y_j}\frac{\partial y_j}{\partial t} \tag{4}$$

The mass balance equations are:

$$\frac{\partial u}{\partial z} = -\frac{\alpha}{P}\frac{\partial P}{\partial t} + \frac{\alpha}{T}\frac{\partial T}{\partial t} + \frac{u}{T}\frac{\partial T}{\partial z} - \frac{RT}{P}\rho_B \sum_{j=1}^{n}\left(H_j + \sum_{k}^{n-1}\frac{\partial q_j}{\partial y_k}\frac{\partial y_k}{\partial t}\right) \tag{5}$$

$$A_i \frac{\partial y_i}{\partial t} - \sum_{\substack{j=1 \\ j\neq i}}^{n-1} B_{ij}\frac{\partial y_j}{\partial t} + u\frac{\partial y_i}{\partial z} + C_i = 0 \quad i = 1, 2, \ldots n-1 \tag{6}$$

where

$$H_j = \frac{\partial q_j}{\partial P}\frac{\partial P}{\partial t} + \frac{\partial q_j}{\partial T}\frac{\partial T}{\partial t}$$

$$A_i = \alpha - y_i \frac{RT}{P}\rho_B \sum_{j}^{n}\frac{\partial q_j}{\partial y_i} + \frac{RT}{P}\rho_B \frac{\partial q_i}{\partial y_i}$$

$$B_{ij} = y_i \frac{RT}{P}\rho_B \sum_{k}^{n}\frac{\partial q_k}{\partial y_j} - \frac{RT}{P}\rho_B \frac{\partial q_i}{\partial y_j}$$

$$C_i = -y_i \frac{RT}{P}\rho_B \sum_{j}^{n} H_j + \frac{RT}{P}\rho_B \sum_{j}^{n} H_j$$

Surface and pore diffusion model

When the mass transfer rates are finite, S_i must be expressed in terms of a mass transfer rate. Here, only diffusion in the pores will be considered since the film diffusion resistance has been shown to be negligibly small as compared to that of pore diffusion for the system being considered (Tsai et al., 1983). Two fluxes contribute to the pore diffusion: surface and gas phase. The significance of surface diffusion has been demonstrated. In a recent demonstration by Costa et al. (1985), up to 70–80% of the total flux is due to surface diffusion for the system of CH_4 in activated carbon at 20°C and pressures below 0.4 atm. Inclusion of the surface flux is not merely to increase the total flux. It also changes the dynamics in the adsorber since surface diffusivity is a strong function of surface coverage (Yang et al., 1973) and hence of the gas concentrations, whereas the pore diffusivity in the gas phase can be assumed to be independent of the gas concentrations.

The mass balance for component i inside the pores of a spherical particle at axial location z yields:

$$\epsilon \frac{\partial C_{iP}}{\partial t} + \frac{1}{r^2}\frac{\partial}{\partial r}(r^2 N_{ir}) + \rho_P \frac{\partial q_i}{\partial t} = 0 \quad i = 1, 2, \ldots n \tag{7}$$

The following particle-volume averaged quantities are introduced to simplify the computation:

$$\bar{C}_{ip} = \frac{3}{a^3}\int_0^a C_{ip} r^2 dr \quad i = 1, 2, \ldots n \tag{8a}$$

$$\bar{q}_i = \frac{3}{a^3}\int_0^a q_i r^2 dr \quad i = 1, 2, \ldots n \tag{8b}$$

By integrating Eq. 7 with respect to r and using the particle-averaged quantities, we have:

$$\epsilon \frac{\partial \bar{C}_{ip}}{\partial t} + \frac{3}{a}(N_i)_{r=a} + \rho_P \frac{\partial \bar{q}_i}{\partial t} = 0 \quad i = 1, 2, \ldots n \tag{9}$$

To further simplify the model, parabolic concentration profiles within the particle are assumed, which are good assumptions when compared with the computed profiles (Tsai et al., 1983).

$$C_{ip} = E_i + F_i r^2$$

where

$$E_i = C_{ip}^s - F_i a^2 \quad i = 1, 2, \ldots n$$

$$F_i = (C_{ip}^s - \bar{C}_{ip})\frac{5}{2a^2} \tag{10}$$

Therefore,

$$\left(\frac{\partial C_{ip}}{\partial r}\right)_{r=a} = (C_{ip}^s - \bar{C}_{ip})\frac{a}{5} \quad i = 1, 2, \ldots n \tag{11}$$

The flux N_{ir} comprises pore and surface diffusion. The pore diffusion is dominated by Knudsen diffusion with a constant diffusivity, D_{ik}. The surface diffusivity is D_{is}, which is a function of the total surface coverage (Yang et al., 1973). Thus we have:

$$N_{ir} = -D_{ik}\frac{\partial C_{ip}}{\partial r} - D_{is}\rho_P \frac{\partial q_i}{\partial r} \tag{12}$$

Inside the pores, $\bar{q}_i$ is a function of T and $\bar{C}_{ip}$ approximated by the equilibrium adsorption. The flux at the pore mouth at the

particle surface is:

$$(N_i)_{r=a} = -D_{ik}\left(\frac{\partial C_{ip}}{\partial r}\right)_{r=a} - D_{is}\,\rho_P \sum_j^n \frac{\partial \bar{q}_i}{\partial \bar{C}_{jp}}\left(\frac{\partial C_{jp}}{\partial r}\right)_{r=a} \qquad i = 1, 2, \ldots n \quad (13)$$

Here T is assumed uniform inside the particle, and $(\partial q_i/\partial C_{jp})_{r=a}$ is approximated by the particle-volume averaged quantity $\partial \bar{q}_i/\partial \bar{C}_{jp}$. Substituting Eqs. 11 and 13 into Eq. 9, we have:

$$\epsilon \frac{\partial \bar{C}_{ip}}{\partial t} - \frac{15}{a^2} D_{ik}(C^s_{ip} - \bar{C}_{ip}) - \frac{15}{a^2} D_{is}\,\rho_P \sum_j^n \frac{\partial \bar{q}_i}{\partial \bar{C}_{jp}}(C^s_{jp} - \bar{C}_{jp}) + \rho_P \frac{\partial \bar{q}_i}{\partial t} = 0 \qquad i = 1, 2, \ldots n \quad (14)$$

where the time derivative of $\bar{q}_i$ is:

$$\frac{\partial \bar{q}_i}{\partial t} = \frac{\partial \bar{q}_i}{\partial T}\frac{\partial T}{\partial t} + \sum_j^n \frac{\partial \bar{q}_i}{\partial \bar{C}_{jp}}\frac{\partial \bar{C}_{jp}}{\partial t} \qquad i = 1, 2, \ldots n \quad (15)$$

The final equation for $\bar{C}_{ip}$ is:

$$\left(\epsilon + \rho_P \frac{\partial \bar{q}_i}{\partial \bar{C}_{ip}}\right)\frac{\partial \bar{C}_{ip}}{\partial t} + \rho_P \sum_{j\neq i}^n \frac{\partial \bar{q}_i}{\partial \bar{C}_{jp}}\frac{\partial \bar{C}_{jp}}{\partial t} - \frac{15}{a^2} D_{ik}(C^s_{ip} - \bar{C}_{ip}) - \frac{15}{a^2} D_{is}\,\rho_P \sum_j^n \frac{\partial \bar{q}_i}{\partial \bar{C}_{jp}}(C^s_{jp} - \bar{C}_{jp}) + \rho_P \frac{\partial \bar{q}_i}{\partial T} = 0 \quad (16)$$

Equation 16 shows that the coupled behavior of the transport of one component is influenced by concentrations of the other components in bulk separation processes. Moreover, the surface diffusivity strongly depends on surface coverage θ, as suggested by the Higashi model (Yang et al., 1973):

$$\frac{D_s}{D_{s,\theta=0}} = \frac{1}{1-\theta} \quad (17)$$

where $\theta = \Sigma\, q_i/V_{mi}$. Obviously the contribution from surface flux increases as surface coverage is increased.

The local sorption rate, S_i, can now be evaluated from Eqs. 11, 13, and 16 as:

$$S_i = \frac{3\rho_B}{\rho_P}\frac{1}{a}(N_i)_{r=a} \quad (18)$$

Since the bed is not nearly isothermal in bulk separation, the following heat balance is written for the bed:

$$(\alpha'\rho_g C_{pg} + \rho_B C_{ps})\frac{\partial T}{\partial t} + \rho_g C_{pg}\, u \frac{\partial T}{\partial z} - \sum_i^n Q_i\,\rho_B \frac{\partial \bar{q}_i}{\partial t} + \frac{2h}{R}(T - T_w) = 0 \quad (19)$$

where α' is the total void fraction, or $\alpha + \epsilon(1-\alpha)$. The last term in Eq. 19 is necessary to account for the heat capacity of the stainless steel wall in the experimental unit since it is relatively large in comparison to the bed. This term may be negligible in commercial units.

The temperature of the wall is:

$$\rho_w C_{pw} A_w \frac{\partial T_w}{\partial t} = 2\pi R h (T - T_w) \quad (20)$$

The boundary conditions for the PSA cycle are:

Step I:

$$y_{H_2}(t, L) = 1,\ T(t, L) = T_o,\ u(t, 0) = 0,\ P = P(t)$$

Step II:

$$y_i(t, 0) = y_{i,o},\ T(t, 0) = T_o,\ u(t, L) = u_L,\ P = P_f$$

Step III:

$$y_i(t, 0) = y_{i,0},\ T(t, 0) = T_o,\ u(t, 0) = 0,\ P = P(t)$$

Step IV:

$$y_i(t, L) = y_i(t', L),\ T(t, L) = T(t', L),\ u(t, L) = 0,\ P = P(t),$$

where t' is at the end of III

Step V:

$$y_{H_2}(t, L) = 1,\ T(t, L) = T_o,\ u(t, L) = u_p,\ P = P_p$$

where the subscripts f and p denote feed and purge, respectively. The pressure history, $P(t)$, as recorded by a pressure transducer, is used as a boundary condition so that the effluent flow rate can be calculated. Alternatively, the effluent flow rate, $u(t)$, may be used as the boundary condition and $P(t)$ can be calculated (Turnock and Kadlec, 1971).

Input information for the models

The following information is needed for the models: equilibrium adsorption, and the pore and surface diffusion coefficients. In addition, the heat transfer coefficient between the bed and the wall is readily evaluated as 3×10^{-3} cal/cm^2 · °C · s (12.6×10^{-3} J/cm^2 · °C · s) (Yagi and Wakao, 1959).

Several methods are available for predicting equilibrium adsorption of mixtures from single-gas isotherms. Two will be employed here: the loading ratio correlation (LRC) and the ideal adsorbed solution theory (IAS). Each will also be modified based on experimental data. LRC is the only noniterative method, which is the Langmuir isotherm extended to n components, except that the Langmuir isotherm is replaced by a hybrid Langmuir-Freundlich equation. The LRC equations are:

$$q_i = \frac{V_{mi} B_i (Py_i)^{b_i}}{1 + \sum_j^n B_j (Py_j)^{b_j}} \qquad i = 1, 2, \ldots n \quad (21)$$

Although not thermodynamically rigorous, the LRC has shown good correlation for zeolites (Yon and Turnock, 1971) and activated carbon (Chen and Yang, 1985). The constants B_i can be modified empirically to account for the lateral interactions on

the surface:

$$B_i' = \frac{B_i}{\eta_i} \tag{22}$$

The constants for H_2, CH_4, and CO_2 on activated carbon in Eq. 21 have been determined by Saunders and Yang (1985), covering the ranges 295–480 K and 0–1,000 psig (0–6.89 MPa). The values of η for the ternary mixture adsorption system have been determined by Ritter (1985). Table 1 summarizes the data. Although the values of η are close to unity, the small deviations have a rather sizable effect on the PSA results, as will be shown shortly.

In the IAS theory (Myers and Prausnitz, 1965), the spreading pressure, π, is given by:

$$\frac{\pi S}{RT} = \int_0^P \frac{q}{p}\, dP \tag{23}$$

where S is surface area, and Raoult's law is assumed for the adsorbed mixture:

$$Py_i = P_i^o(\pi)x_i \quad i = 1, 2, \ldots n \tag{24}$$

where $P_i^o(\pi)$ is the vapor pressure for the pure i adsorbed at the same T and π of the adsorbed mixture. When the Langmuir isotherm applies to the single gases, which is approximately correct for the system in this study, Eq. 23 can be integrated, and P_i^o can be expressed in terms of π. Combining the integrated P_i^o and Eq. 24 gives:

$$\sum_i^n \frac{Py_i}{p_i^o} = \sum_i^n \frac{Py_i B_i}{\exp\left(\dfrac{\pi S}{RTV_{mi}}\right) - 1} = 1 \tag{25}$$

For a given P and gas composition, Eq. 25 is solved for π, and Eq. 24 then yields x_i. However, a trial and error procedure is needed for solving Eq. 25. Surprisingly, the IAS and LRC methods give very similar results in all cases tested in this laboratory (Chen and Yang, 1984; Ritter, 1985).

Both methods will be used in the PSA models. For a fair comparison, the empirical B_i' values will be used in Eq. 25.

For the pore (Knudsen diffusion dominates under our conditions) and surface diffusivities, empirical tortuosity factors are needed. Although the tortuosity factors for the two effective diffusitivies may be different, the same factor will be used.

The activated carbon (PCB, Calgon Corp., Pittsburgh) has a monodisperse pore size of 1.6 nm dia. The diffusivities of O_2/He and N_2/He at 25°C and 1 atm (101.3 kPa) were measured at Calgon (Liu, 1984) using a transient technique (Yang and Liu, 1982), giving 2×10^{-5} and 2.5×10^{-5} cm^2/s, respectively. Comparing these effective values with the Knudsen diffusivities, a mean tortousity of 65 is obtained. For surface diffusivity, the correlation by Sladek et al. (1974) is used:

$$D_{A,\theta=0} = 1.6 \times 10^{-2} \exp\left(-0.45\, Q/mRT\right) \tag{26}$$

The value of m is 1 for physical adsorption on carbon. The effective surface diffusivity for CH_4 on activated carbon, under low-coverage conditions at 20°C, was measured as 9.1×10^{-6} cm^2/s (Costa et al., 1985). The tortuosity for surface diffusion, given by the ratio of the value from Eq. 26 to the experimental value, is 37.

A mean tortuousity factor of 50 will be used for both Knudsen and surface diffusion. Thus, the effective surface diffusivities for CH_4, CO_2, and H_2 are, respectively, 7.4×10^{-6}, 7.4×10^{-6}, and 3.8×10^{-5} cm^2/s. The effective Knudsen diffusivities are 4.2×10^{-5}, 2.5×10^{-5}, and 1.2×10^{-4} cm^2/s, respectively.

Table 1. Parameters Used in Loading Ratio Correlation Equation for Adsorption on PCB Activated Carbon

	k_1	k_2	k_3	k_4	b_i	η_i	Q_i
CH_4	9.67 E-3	−1.25 E-5	3.8 E-5	1,731.3	1.0	1.2	5,000
CO_2	1.69 E-2	−2.49 E-5	3.67 E-5	1,892.6	1.0	0.84	5,000
H_2	1.47 E-2	−1.39 E-5	4.23 E-6	1,227.5	0.96	1.08	2,800

$V_{mi} = k_1 + k_2T$.
$B_i = k_3 \exp(k_4/T)$.
T in K.
P in psig (kPa = psia × 6.89).
Q_i = heat of adsorption, cal/mol (J = cal × 4.19).

Method of solution

The two models are numerically solved by employing finite-difference methods. The packed bed is divided into 40 equal-volume cells where the concentrations are uniform within each cell. Time intervals as small as 0.1 s are used, depending on the sharpness of the concentration wave fronts, to assure stability and accuracy of the solution.

For the equilibrium model, Eq. 6 is first solved for each cell and time step. Equation 6 represents $n - 1$ ODE's with $n - 1$ unknowns, $\partial y_i/\partial t$. A standard Gaussian elimination method is used to solve these equations. With the values of $\partial y_i/\partial t$, Eq. 5 is integrated to obtain the superficial velocity u at different bed locations. In Eq. 6 the coefficients containing the q_i derivatives have isotherm and bed properties. These coefficients are evaluated by numerical differentiation using the conditions in the previous time step. Therefore, an explicit scheme is actually used for solving Eqs. 5 and 6. The energy balance equations, Eqs. 19 and 20, are solved in a similar manner by an explicit finite-difference scheme, using the values of $\partial \bar{q}_i/\partial t$ evaluated from Eq. 4.

For solving the pore and surface diffusion model, Eq. 16 is first recast into a semi-implicit finite-difference form:

$$\sum_j^n G_{ij}\, \bar{C}'_{jP} = H_{ij}\, \bar{C}_{jP} - F_{ij} \quad i = 1, 2, \ldots n \tag{27}$$

where

$$G_{ij} = \delta_{ij}\left(\epsilon + \frac{\Delta t}{2}\frac{15}{a^2} D_{ik}\right) + \left(1 + \frac{\Delta t}{2}\frac{15}{a^2} D_{is}\right)\rho_p \frac{\partial \bar{q}_i}{\partial \bar{C}_{jP}}$$

$$H_{ij} = \delta_{ij}\left(\epsilon - \frac{\Delta t}{2}\frac{15}{a^2} D_{ik}\right) + \left(1 - \frac{\Delta t}{2}\frac{15}{a^2} D_{is}\right)\rho_p \frac{\partial \bar{q}_i}{\partial \bar{C}_{jP}}$$

$$F_{ij} = \Delta t \frac{15}{a^2}\frac{y_i P}{RT}\left(\delta_{ij} D_{ik} + \rho_p D_{is}\frac{\partial \bar{q}_i}{\partial \bar{C}_{jP}} + \Delta t\, \rho_p \frac{\partial \bar{q}_i}{\partial T}\right)$$

and δ_{ij} is the Kronecker delta

$$\delta_{ij} = 1 \text{ for } i = j$$

$$\delta_{ij} = 0 \text{ for } i \neq j$$

In Eq. 27, the pore concentration at the exterior surface of the particle, C^s_{ip}, has been replaced by the interparticle concentration, $y_i P/RT$. Equation 27 is a set of n algebraic equations used to evaluate the n concentrations at the next time step, $\overline{C}'_{jP}$. The coefficients in these equations contain diffusivities (Knudsen D_{ik} and surface D_{is}) and isotherm properties, $\partial \overline{q}_i/\partial \overline{C}_{jP}$ and $\partial \overline{q}_i/\partial T$, which are calculated by numerical differentiation of LRC or IAS. Equation 27 is solved by the Gaussian elimination method. With the aid of Eqs. 11 and 13, S_i is calculated from Eq. 18. The superficial velocity, u, at all locations in the bed is then calculated by integrating Eq. 2 with respect to z. Since the influence of $\partial T/\partial t$ and $\partial T/\partial z$ on u is substantially smaller than that by $\partial P/\partial t$ and S_j, the temperature derivatives are evaluated at the previous time step. Equation 3 is finally solved by recasting it into a semi-implicit finite-difference form:

$$\alpha \frac{y'_i - y_i}{\Delta t} + u_i \frac{(y'_i - y'_{i-1}) + (y_i - y_{i-1})}{2\Delta z} + \frac{RT}{P} \frac{y'_i + y_i}{2} \sum_j^n S_j - S_i = 0 \quad (28)$$

where the superscript prime denotes the value at the end of a time step, and subscript i denotes the ith cell in the column. Equation 28 is solved for each component in the mixture. Since it is in a linear form with respect to y'_i, it is solved directly with the known values of y_i, y'_{i-1}, and y_{i-1}. The energy balance equations 19 and 20, are solved in the same manner as the equilibrium model.

Using a VAX 780 minicomputer, and with 40 space steps, and 7,200 time steps (0.1 s for each time step), the pore and surface diffusion model requires approximately 10 min of computation time for each PSA cycle, not an excessive amount of time.

Experimental

The experimental apparatus, shown in Figure 2, was designed for simulating all basic steps involved in PSA processes and was

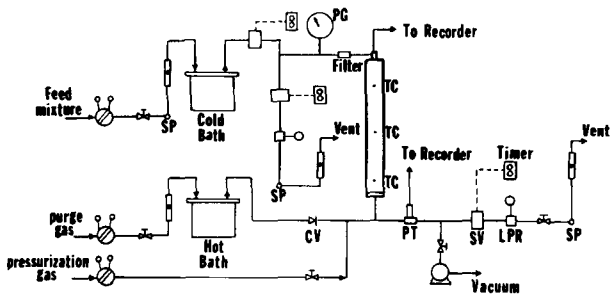

Figure 2. Diagram of apparatus for pressure swing adsorption for gas separation.

SP, sampling port
PG, pressure gauge
CV, check valve
PT, pressure transducer
SV, solenoid valve
TC, thermocouple
LPR, line pressure regulator

Table 2. Adsorption Bed Characteristics

Bed inside radius, R = 2.05 cm
Bed length, L = 60 cm
Particle size, a = 0.028 cm
Bulk density, ρ_B = 0.498 g/cm^3
Particle density, ρ_p = 0.85 g/cm^3
Interparticle void fraction, α = 0.43
Intraparticle void fraction, ϵ = 0.61
Total void fraction = 0.78
Heat capacity of carbon, C_{ps} = 0.25 cal/g · °C
Heat capacity of wall, C_{pw} = 0.11 cal/g · °C
Avg. C_p of gas mixture, C_{pg} = 7.647 cal/gmol · °C

SI conversion: J = cal × 4.184.

capable of a wide range of operating conditions. The details have been described elsewhere (Yang and Doong, 1985). A ternary mixture of $H_2/CH_4/CO_2$, at one-third volume fraction each, was separated. The adsorbent was 20–60 mesh (mean radius = 0.028 cm) PCB activated carbon, manufactured by Calgon Corporation. The adsorber characteristics are listed in Table 2.

All solenoid valves were controlled by preset electric timers, Figure 2. The process operation was automated. The effluent flow rate and its composition were sampled and recorded at desired time intervals. The adsorber bed was cleaned prior to each PSA run by prolonged degassing with a mechanical pump. The run was initiated with H_2 pressurization, step I, where H_2 was fed from the lower end of the bed. The high-pressure feed, step II, followed immediately from the upper end of the bed. The flow rate in step II was controlled by adjusting a needle valve in the effluent (at nearly ambient pressure) line. Cocurrent depressurization, step III, was effected by closing the feed valve. Countercurrent blowdown, step IV, was achieved by simultaneously closing the bottom valve and opening the top valve. When the column pressure dropped to a certain level, a check valve opened, which initiated the H_2 purge step.

One-half minute was used for step I and 3 min for step II in all experiments. The duration of step III ranged from 5 to 8 min, and that of steps IV and V from 2 to 4 min. There was no distinction between steps IIIa and IIIb in the operation, but two product cuts were taken from the same step. The highest feed pressure was 300 psig (2.07 MPa). The feed rate was in a range from 6 to 12 LSTP/min during step II. A cyclic steady state was generally reached after 10 cycles from start-up with a clean bed.

In commercial PSA operations, step I may be replaced by several pressure equalization steps where impure H_2 products from other beds are used. The effects of the H_2 purity used in step I on the separation results are not strong (Cen and Yang, 1986). Thus, the feed mixture was also used in this step, and gave good separations (Yang and Doong, 1985).

Results and Discussion

It has been previously demonstrated that two high-purity products can be obtained by PSA from a binary mixture (Yang and Doong, 1985). For mixtures containing more than two components, however, the feasibility of obtaining high-purity products for all components has not been demonstrated by using a single PSA unit. The process by Sircar (1979), which used two sorbents and two bed batteries, produced two high-purity products from a ternary mixture. The first goal of the experimental program using a single sorbent and one bed was to demonstrate

that two (and possibly three) high-purity products can also be recovered from a ternary mixture. The surface/pore diffusion model was then verified by the experimental data. The importance of surface diffusion was demonstrated (due to the high surface coverage in PSA), and contributed to over 50% for the total flux in the pores. This study also provided a basic understanding of the dynamics of PSA separation in a multicomponent mixture.

Results of a typical run

The feed mixture, as in all runs, contained 33.33% by volume each of H_2, CH_4, and CO_2. Using the five-step PSA cycle described, the following products were recovered: high-purity H_2 from step II or steps II and IIIa, high-purity CH_4 from step IIIb, and a CO_2-rich product from steps IV and V. The results of a typical run (run 1 in later discussion) are shown in Table 3, and display the raw data from a steady-state cycle. This run was conducted at a feed pressure of 100 psig (0.79 MPa), with a total throughput of 21 LSTP feed for a 12 min cycle. The effluent from step II, which lasted 3 min, was a high-purity H_2 product. With the feed closed at the end of step II, H_2 recovery continued during depressurization, step IIIa. Due to the sharp concentration wave front of CH_4 in the bed, a CH_4 product was recovered in the late stage of bed depressurization, step IIIb. In this run, step IIIb lasted 4.5 min. The CH_4 product purity was nearly 90%. The countercurrent blowdown and purge steps produced a CO_2-rich gas, which was only 60% pure due to the large amount of CH_4 in the CO_2-covered region. The poor separation between CH_4 and CO_2 was a direct consequence of the low selectivity (or separation factor) of the pair on activated carbon. The selectivity, expressed in $(x_2/y_2)/(x_1/y_1)$, where subscript 2 = CO_2 and 1 = CH_4, was nearly two. The selectivity of CH_4 over H_2 for the same sorbent was nearly 10. In a forthcoming study we show that it is not possible to separate binary CH_4/CO_2 mixtures into high-purity product by using activated carbon in PSA (Doong and Yang, 1986). It is likely that with a higher selectivity, e.g., by using a zeolite sorbent, a high-purity CO_2 product is also possible. The low selectivity of CO_2 over CH_4 on activated carbon made it difficult to obtain a high-purity CO_2 product; it also lowered the CH_4 recovery. The CH_4 recovery in this run was 32%. Nonetheless, the PSA cycle used here could also be used to obtain three high-purity products from a ternary mixture, with the proper selection of sorbent giving reasonable selectivities.

Table 3. Typical Experimental Results, Run 1 in a Steady State Cycle for PSA Separation of Equimolar Mixture of CH_4, CO_2, and H_2

Step	Time s	CH_4 %	CO_2 %	H_2 %	Effl. Flow Rate L/min at STP
II (3 min)	30	0.2	0.1	99.7	3.0
	90	0.3	0.1	99.6	3.0
	150	0.5	0.1	99.4	3.0
IIIa (2 min)	210	2.7	0.1	97.2	2.3
	255	9.0	0.1	90.9	1.3
	295	11.8	0.2	88.0	0.8
IIIb (4.5 min)	315	74.0	1.0	25.0	0.6
	360	85.3	1.2	13.5	0.6
	420	92.1	1.3	6.6	0.6
	480	92.5	1.4	6.1	0.6
	540	93.5	1.5	5.0	0.5
IV, V (2 min)	585	38.5	61.5	0.0	7.8
	615	38.5	61.0	0.5	5.5
	645	36.5	49.7	13.8	5.8
	675	36.5	42.0	21.5	6.1

Pressure history is shown in Figure 3.

The product recovery was calculated as the ratio between the amount of component in the product stream to that in the feed. The recoveries for H_2 and CO_2 were 83 and 99%, respectively. The recovery for H_2 was only 83% because the H_2 used in bed repressurization and purge was not considered a useful product.

Effect of end pressure of cocurrent depressurization

Cocurrent depressurization was used to increase H_2 recovery, and to enrich CH_4 product. The important role played by this step in increasing concentrations of the strongly adsorbed components has been explained in detail by a bed loading analysis (Yang and Doong, 1985). It was illustrated that during this step H_2 was eluted out of the mass transfer zones, and total loading of the strongly adsorbed component was increased. However, an adverse effect arose from this step. Since "favorable" adsorption isotherms were used, i.e., concave type, the wave fronts of CH_4 and CO_2 would continue to broaden as they propagated through the column (Ruthven, 1984). Consequently, these diffuse wavefronts would cause poor separations. When the end pressure of this step was lowered, the CO_2 contamination in the CH_4 product became worse. These effects are shown in the steady state PSA results in Figures 3 and 4, along with the pressure histories. Runs 1 and 2, and runs 3 and 4 were comparable, with similar operating conditions with the exception of the end pressure of step III. The undesirable and early breakthroughs of CH_4 and CO_2, caused by lowering the end pressure, were clearly seen in these figures. The integrated results of these runs are shown in

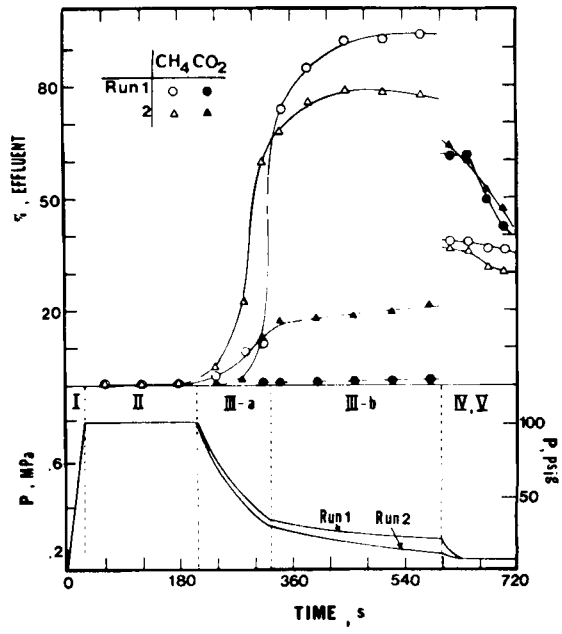

Figure 3. Experimental effluent concentrations and pressure histories in a steady state PSA cycle for runs 1 and 2.
(See Table 4 for conditions.)

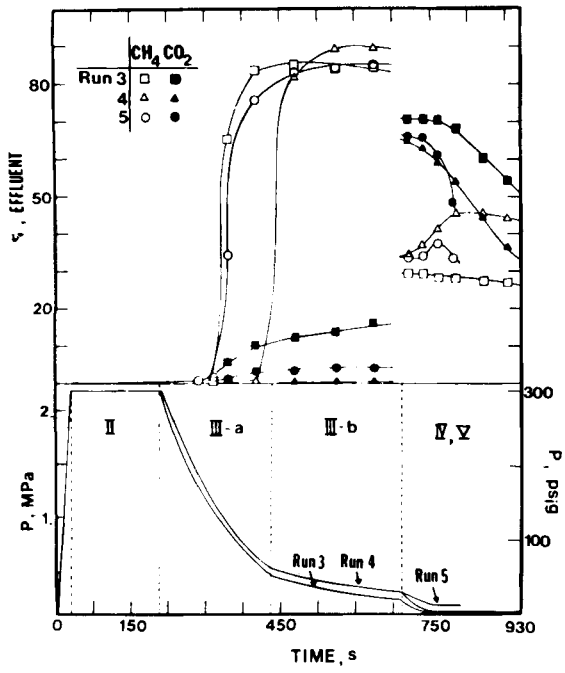

Figure 4. Experimental effluent concentrations and pressure histories in a steady state PSA cycle for runs 3–5.
(See Table 5 for conditions.)

Tables 4 and 5. The feed amounts of all components are also shown in the tables. These feed amounts were calculated from the effluents in all steps in the steady state cycle by mass balance. Since the amount of H_2 purge was measured, the H_2 used in pressurization was calculated from the total H_2 feed.

Effect of the purge pressure

At the same feed pressure, the effect of the purge pressure has also been referred to as pressure ratio, i.e., adsorption pressure/purge pressure (Chan et al., 1981). A major conclusion in the study of a binary mixture by Chan et al. was that the critical purge/feed ratio required for a given purity of the weakly adsorbed (from step II) decreased with the increasing pressure ratio. This finding was a direct consequence of the degree of bed cleaning. At the same feed pressure, a lower purge pressure would result in a cleaner bed, and hence a higher H_2 product purity. The same effect was observed in this work. Table 5 illustrates an example by comparing runs 4 and 5. The purge/feed ratio and other conditions were approximately the same for the two runs, except the purge pressure. The lower purge pressure yielded a higher H_2 purity as well as CH_4 purity. On the other hand, the CO_2 product purity was lowered since more CH_4 was eluted in the purge step, as seen in Figure 4. The pressure histories and the steady state effluent concentrations are shown in Figure 4. In run 5, the purge time was shortened because the purge flow rate was higher than in run 4, and the purge/feed ratio was to be maintained.

Effect of purge/feed ratio

The effect of the purge/feed ratio on the purity of the weakly adsorbed component (product in step II) has been studied by many groups. The product purity increases with the purge/feed ratio in an asymptotic manner; beyond a certain range of purge/feed ratio the purity levels off. A higher purge/feed ratio is not desirable because it dilutes the product purity of the strongly adsorbed component(s), and it lowers the product recovery of the weakly adsorbed component. For bulk separations of binary mixtures, it was found that the range from 0.06–0.08 was optimum for purge/feed (Yang and Doong, 1985). The purge/feed ratio is most rationally defined as amount of purge/amount of feed, measured at the same conditions. The effect of purge/feed is less important at high pressure ratios since the bed is relatively clean by low-pressure desorption (Yang and Doong).

For ternary mixture separation where all components are desired products, the effect of the purge/feed ratio is a more complicated one. However, the same basic relationship applies. Runs 6 and 7 were made under similar conditions except for the purge/feed ratio, which was doubled in run 7. The purge/feed ratio was 0.072 in run 6. The steady state effluent characteristics are shown in Figure 5; the integrated results are in Table 6. It should be noted that in most of the published literature feed mixture was used in bed repressurization, whereas H_2 was used in this study. The effect of the purge/feed ratio should be diminished. As shown in Table 6, the H_2 purity was slightly higher in step II, and substantially higher in step IIIa due to the later breakthrough of CH_4 (Figure 5). The higher purge amount in run 7 also diluted the CO_2 product.

Table 4. Overall Separation Performance of PSA in a Steady State Cycle; Effect of End Pressure of Cocurrent Blowdown Step

	Run 1				Run 2			
Step	Output L	CH_4	CO_2	H_2	Output L	CH_4	CO_2	H_2
II	9.0	0.3	0.1	99.6	8.81	0.2	0.3	99.5
IIIa	3.3	5.0	0.1	94.9	2.8	13.2	2.2	84.6
IIIb	2.6	88.8	1.3	9.9	3.9	76.8	19.4	3.7
IV, V	12.69	37.5	54.0	8.5	10.4	33.2	56.3	10.5
Purge Amount		2.2				2.0		
End pressure of IIIb		20 psig (239.1 kPa)				12 psig (184.0 kPa)		
Total feed per cycle		21.1				20.3		
Amt H_2 in pressurization		4.2				3.6		

See Figure 3.
Concentrations are in mol %, amounts are in LSTP.

Table 5. Separation Performance of PSA in a Steady State Cycle; Effects of End Pressure of Cocurrent Blowdown Step (Runs 3, 4) and Pressure Ratio (Runs 4, 5)

	Run 3				Run 4				Run 5			
Step	Output L	CH_4	CO_2	H_2	Output L	CH_4	CO_2	H_2	Output L	CH_4	CO_2	H_2
II	17.1	0.0	0.1	99.9	17.1	0.1	0.0	99.9	16.8	0.1	0.1	99.8
IIIa	8.6	5.4	0.7	93.9	10.6	0.3	0.1	99.6	7.8	3.5	0.3	96.2
IIIb	8.0	84.5	13.0	2.5	3.6	87.2	0.8	12.0	5.9	82.5	3.9	13.6
IV, V	14.5	28.3	66.2	5.5	19.6	39.9	55.8	4.3	16.7	34.6	61.5	4.3
Purge amount		1.8				1.9				1.5		
Purge pressure		3 psig (122 kPa)				3 psig (122 kPa)				12 psig (184 kPa)		
End pressure of IIIb		20 psig (239 kPa)				32 psig (322 kPa)				32 psig (322 kPa)		
Total feed per cycle		33.1				33.0				32.3		
Amt H_2 in pressurization		13.3				16.0				13.6		

See Figure 4.
Concentrations are in mol %, amount are in LSTP.

Effect of feed rate

The effect of feed rate can be discussed more rationally as the effect of bed utilization or bed coverage in step II of the cycle. A longer bed coverage in step II (or shorter unused bed length), as a result of a higher feed rate at the same cycle time, will result in earlier breakthroughs of the adsorbed components and hence will lower the purity of the light product. A longer bed coverage also leaves a shorter clean bed for readsorption of the heavier components during step III, which is also undesirable. The above relationships were illustrated by runs 8 and 9, and Table 7, at the same purge/feed ratio and other conditions except the feed rate. The pressure history was similar to that in run 4, except the end pressure of step III was 26 psig (0.28 MPa) (Figure 4). The feed rates differed by approximately 10% in these runs. (To have a greater difference the "optimal" operating conditions would have to be changed.) The higher feed rate gave an earlier CH_4 breakthrough in step III (run 9, Table 7) for the reasons described in the foregoing. However, the CO_2 product purity was increased by a greater feed amount.

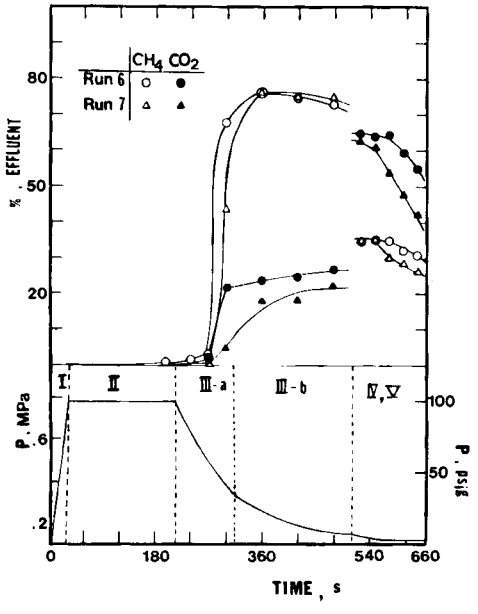

Figure 5. Experimental effluent concentrations and pressure histories in a steady state PSA cycle for runs 6 and 7.
(See Table 6 for conditions.)

Comparisons between models and experiments

A typical comparison between the experimental data and the models will be shown for runs 1 and 2. The cyclic steady state effluent concentrations are compared in Figures 6 and 7. (The pressure histories are shown in Figure 3). The LRC equations were used in all model simulations unless stated otherwise. Three models were compared: the equilibrium model, the pore diffusion model considering only Knudsen diffusion ($D_{is} = 0$), and the pore diffusion model considering both Knudsen and surface diffusion. As in all other runs, the pore diffusion model considering both Knudsen and surface diffusion best described the experimental data. The equilibrium model predicted a later breakthrough for both CH_4 and CO_2 (due to the assumption of infinite pore diffusion rate), plus a higher CH_4 concentration and a lower CO_2 concentration in step III.

As mentioned, surface diffusion can make a substantial contribution to the total flux in pores under conditions where surface concentration is high. This has been demonstrated by Costa et al. (1985) in their flux measurement of CH_4 in activated carbon at pressures lower than those in this study, where up to 80% of the total flux was due to surface diffusion. The importance of surface diffusion in the cyclic PSA process will be shown by a comparison of the two pore diffusion models: Knudsen diffusion alone, and both Knudsen and surface diffusion. The comparison shown in Figures 6 and 7 clearly indicates the inadequacy of the Knudsen diffusion model. However, the Knudsen diffusivities were obtained from a tortuosity estimated from literature data. The results using arbitrarily low tortuosities are also shown in Figure 6. The results using tortuosities of 5 and 10 (rather than the estimated 50) show that the experimental results cannot be predicted adequately by using a high Knudsen pore diffusivity. Knudsen diffusivity does not depend on surface concentration

Table 6. Separation Performance of PSA in a Steady State Cycle; Effects of Purge Amount

Step	Run 6 Output L	Run 6 CH_4	Run 6 CO_2	Run 6 H_2	Run 7 Output L	Run 7 CH_4	Run 7 CO_2	Run 7 H_2
II	8.8	0.3	0.5	99.2	8.9	0.2	0.3	99.5
IIIa	3.5	13.6	5.4	81.0	2.4	5.2	1.3	93.5
IIIb	4.2	74.5	25.5	0.0	5.4	75.5	20.0	4.5
IV, V	8.3	33.7	62.1	4.2	10.4	30.8	53.5	15.7
Purge amount		1.4				2.8		
End pressure of IIIb		12 psig (184 kPa)				12 psig (184 kPa)		
Total feed per cycle		19.4				21.2		
Amt H_2 in pressurization		4.0				3.2		

See Figure 5.
Concentrations are in mol %, amounts are in LSTP.

Table 7. Separation Performance of PSA at Steady State; Effects of Feed Rate

Step	Run 8 Output L	Run 8 CH_4	Run 8 CO_2	Run 8 H_2	Run 9 Output L	Run 9 CH_4	Run 9 CO_2	Run 9 H_2
II	17.1	0.0	0.0	100.0	19.1	0.0	0.1	99.9
IIIa	8.7	3.7	0.2	96.1	9.6	12.4	1.8	85.8
IIIb	6.9	78.5	3.9	17.6	7.1	78.2	12.8	9.0
IV, V	16.3	32.2	60.3	7.5	16.5	30.2	64.4	5.4
Purge amount		1.2				1.8		
End pressure of IIIb		32 psig (322 kPa)				32 psig (322 kPa)		
Total feed per cycle		31.6				35.1		
Amt H_2 in pressurization		16.1				14.2		

See run 4, Figure 4 for pressure histories.
Concentrations are in mol %, amounts are in LSTP.

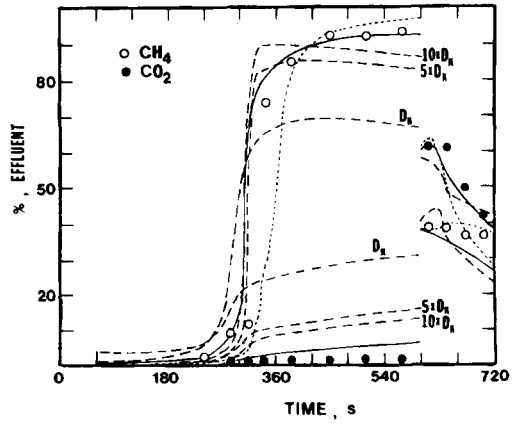

Figure 6. Comparison of effluent concentrations between experimental and predicted results in a steady state cycle for run 1.
O ● experimental
—— surface and Knudsen diffusion model
– – – Knudsen diffusion model
------ equilibrium model

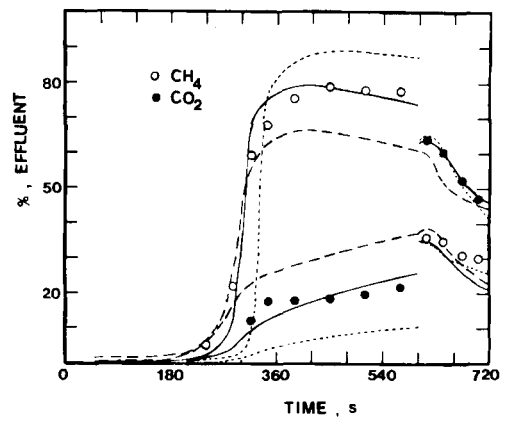

Figure 7. Comparison of effluent concentrations between experimental and predicted results at steady state for run 2.
O ● experimental
—— surface and Knudsen diffusion model
– – – Knudsen diffusion model
------ equilibrium model

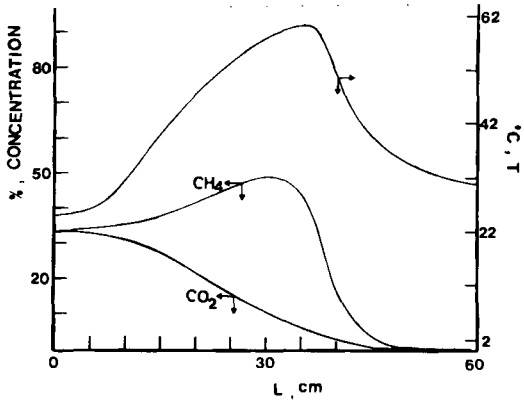

Figure 8. Steady state concentration and temperature profiles for run 8 at end of adsorption step, predicted by surface and Knudsen diffusion model.

L is distance from feed end of column.

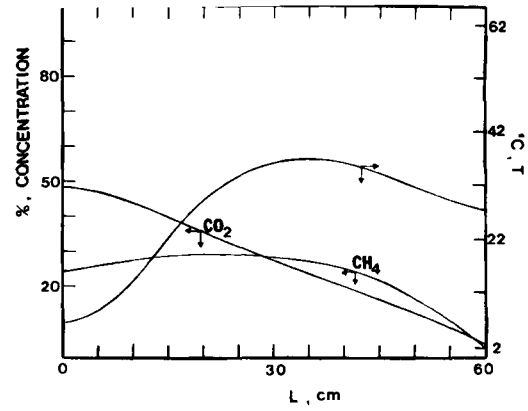

Figure 10. Steady state concentration and temperature profiles for run 8 at end of purge step, predicted by surface and Knudsen diffusion model.

L is distance from feed end of column.

(or amount adsorbed). Surface diffusivity, in contrast, has a strong dependence on surface concentration, which has been corrected and included in the model. The surface diffusion flux, comparing the two flux terms in Eq. 16, is comparable to the Knudsen flux.

The results in steps IV and V were not very sensitive to the different models used. The equilibrium model, however, predicted an earlier CO_2 breakthrough while the Knudsen diffusion model predicted a low CO_2 concentration and a high CH_4 concentration.

The cyclic steady state bed profiles for concentration and temperature computed from the surface diffusion–Knudsen diffusion model are shown in Figures 8 to 10. The agreement between the model simulations and the experimentally observed quantities (effluent concentrations and bed temperatures at three locations) was acceptable at least qualitatively, if not quantitatively, considering the complexities of the process. The profiles shown in these figures helped to provide a basic understanding of the dynamics of the PSA process.

The profiles shown in Figure 8 may be discussed in conjunction with the literature results on breakthrough of multicomponent mixtures in adsorbers. The roll-over or roll-up phenomenon was seen for the CH_4 concentration profile. (This phenomenon, along with cocurrent depressurization, was used to obtain a CH_4-rich product.) In studying adiabatic breakthrough curves for CO_2-C_2H_6-N_2 in a 5A zeolite bed (Basmadjian and Wright, 1981; Liapis and Crosser, 1982), three distinct wave fronts were observed, as predicted by an intracrystal diffusion model. For a concentrated CO_2 and C_2H_6 feed, the first wave front (as seen in breakthrough) was C_2H_6 followed by CO_2, and later, one due to a temperature wave front. The three wave fronts were separated by four plateaus. In Figure 8, the three wave fronts did exist but were not sharp or clearly separated; also, no plateaus could be clearly identified. The major reason for the difference in these two results was that those in Figure 8 were from a cyclic steady state in the PSA process, when the bed was contaminated with a certain amount of preadsorbed CO_2 and CH_4 that was distributed throughout the bed. (More distinct, steeper wave fronts and plateaus were seen from the first few cycles).

The roll-up phenomenon combined with the cocurrent depressurization step was used to enrich the CH_4 product concentra-

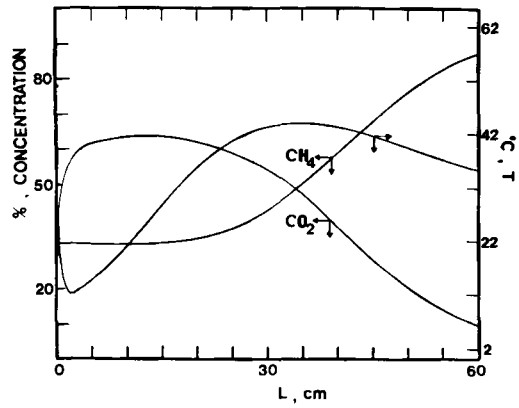

Figure 9. Steady state concentration and temperature profiles for run 8 at end of cocurrent blowdown step, predicted by surface and Knudsen diffusion model.

L is distance from feed end of column.

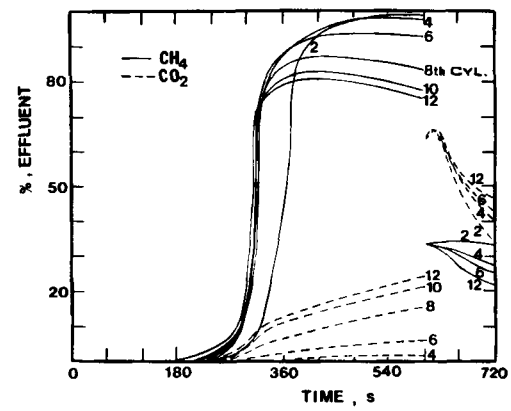

Figure 11. Transient behavior of PSA cycles showing the effluent concentrations in each cycle.

Results are predicted by surface and Knudsen diffusion model for run 2. ____ CH_4, ----- CO_2.

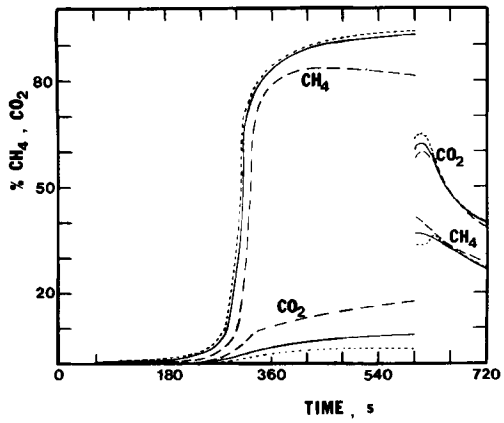

Figure 12. Comparison of effluent concentrations predicted by using different methods for predicting equilibrium mixed gas adsorption.

—— LRC with interaction parameter η_i
------ IAS with interaction parameter η_i
—— LRC without η_i
Results are predicted by surface and Knudsen diffusion model for run 1 in a steady state cycle.

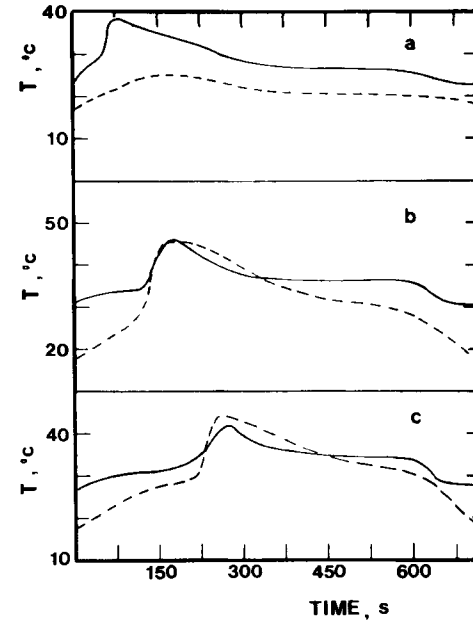

Figure 13. Steady state temperature histories for run 2 at (a) 12.7 cm, (b): 33.0 cm, and (c) 53.3 cm, from top of bed (60 cm height).

—— predicted by the Knudsen and surface diffusion model
---- experimental

tion to nearly 90% in Figure 9. Also in this figure, a minimum temperature near the inlet indicated desorption in the region, whereas a hot zone downstream indicated readsorption of CH_4 and CO_2. In Figure 10, the temperature near the CO_2 product outlet dropped to 10°C due to desorption, and CO_2 concentration was increased. This figure also shows the amount of contamination remaining before the next cycle.

Transient behavior

The major difference between the literature results on adsorber breakthrough curves and the PSA behavior is due to the adsorbed amount that has accumulated in the bed at a cyclic steady state. Figure 11 shows the transient behavior for run 2 from start-up with a clean bed. Approximately ten cycles were required to reach steady state. The CO_2 concentration increased substantially, and undesirably, in the CH_4 product while approaching steady state. In steps IV and V, the CO_2 curve became less steep, while CH_4 was sharpened. These transient behaviors were due to the gradual buildup of contamination. Similarly, it has been observed that preadsorption (Nakao and Suzuki, 1983) and a low purge/feed ratio (Shendalman and Mitchell, 1972) both decreased the number of cycles required to reach steady state.

Isotherms used in PSA modeling

The LRC equations with empirical interaction parameters (η_i) were used in our models. The predictions for equilibrium adsorption from mixtures using the IAS theory and the LRC equations, without empirical correction factors, were surprisingly close (Chen and Yang, 1985). In the PSA model with Knudsen and surface diffusion, the IAS theory was also utilized and compared with the LRC equations, as shown in Figure 12. The IAS theory was modified by using the Langmuir constants, which included the empirical parameters, η_i, Eq. 22. The steady state PSA results using the two different models were indeed very close, both in fair agreement with experimental data. The results incorporating the LRC equations, and without the em-

Table 8. Theoretical Separation Performance of PSA at Steady State Under Conditions in Various Thermal Modes

	Isothermal				Nonisothermal				Adiabatic			
Step	Output L	CH_4	CO_2	H_2	Output L	CH_4	CO_2	H_2	Output L	CH_4	CO_2	H_2
II	17.7	0.1	0.0	99.9	17.4	0.1	0.0	99.9	16.7	0.0	0.1	99.9
IIIa	10.1	0.7	0.0	99.3	9.0	3.0	0.1	96.9	9.8	22.9	1.4	75.7
IIIb	1.3	16.4	0	83.6	2.9	89.9	0.6	9.5	2.4	82.6	9.6	7.8
IV, V	21.3	43.5	49.7	6.8	18.4	37.6	54.6	7.8	13.7	31.2	59.1	9.7
Purge amount		2.0				2.0				2.0		
Total feed per cycle		34.2				32.3				27.7		
Amt H_2 in pressurization		15.1				14.4				13.9		

See run 4, Figure 4 for pressure histories.
Concentrations are in mol %, amount are in LSTP.

pirical parameters or $\eta_i = 1$, showed a significant deviation. This comparison showed the importance of using an accurate isotherm correlation for the PSA modeling. Although the LRC and IAS correlations gave similar results, the computation time for the PSA model using IAS was approximately 70% longer than that using LRC. This was due to the iteration required to find the value of spreading pressure in IAS.

Effects of temperature excursion and particle size on PSA

The main feature in bulk separation by PSA, in contrast to purification, is the large temperature excursions encountered during each cycle. In the experimental unit, the thick stainless wall and the small inside diameter made the process nonadiabatic. A temperature excursion between 5 and 60°C during each cycle was observed in high feed pressure runs. The steady state temperature swing at three locations in the bed for run 2 is shown in Figure 13 along with model predictions by the pore/surface diffusion model. Although not good quantitatively, the main features of the temperature swing were in agreement with the model. The temperature excursion is undesirable for separation. A model comparison of three models, isothermal, adiabatic, and nonisothermal allowing heat exchange with the wall, was made and is shown in Table 8. Although it was difficult to compare results that were not based on optimal conditions, it was clear that the isothermal case yielded the best separation, while the adiabatic case, which was close to commercial operations with large beds, gave the worse results. Two techniques have been suggested to remedy the adverse effects by the temperature swing: allowing heat exchange between beds, and using inert additives with high heat capacities (Yang and Cen, 1986).

By simulation, using the Knudsen-surface diffusion model, the effects of sorbent particle size were also studied and compared with the case that had no mass transfer limitation or equilibrium model. The comparison is shown in Figure 14. According to the model simulation results, the process using a sorbent with a particle radius below 0.014 cm would approach the equilibrium model predictions. The effects of mass transfer limitation were important only in steps II and III. This was unimportant in the blowdown step because the convective flux dominated as a result of the drop in pressure.

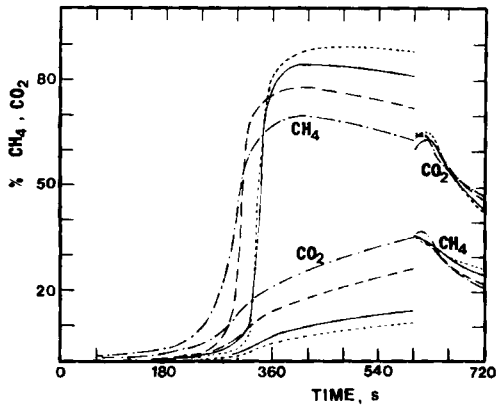

Figure 14. Effects of particle size on steady state effluent concentrations of PSA.

—— a = 0.014 cm
---- a = 0.028 cm
-·- a = 0.056 cm
Results are predicted by surface and Knudsen diffusion model for run 2 at steady state. Also shown: (————) results predicted by equilibrium model.

The effect of H_2 purity in pressurization and purge was studied by model simulation. Using the H_2 product from step II to feed the subsequent steps V and I, no significant differences were seen, as compared with the case using pure H_2. Similar comparisons were observed for 99% H_2. A drop of less than 2% resulted in the CH_4 and CO_2 product concentrations when 95% H_2 was used.

Acknowledgment

This work was supported by U.S. Department of Energy under Grant No. DE-AC21-83MC20183.

Notation

a = average radius of sorbent particle, cm
A = cross-sectional area, cm^2
B = a constant related to the net enthalpy, ΔH, of adsorption according to Langmuir theory, MPa^{-1}
C = concentration of sorbate in bulk flow, mol/L
C_p = heat capacity, cal/mol·K
D_e = effective diffusivity of sorbate, cm^2/min or cm^2/s
$D_{k,s}$ = Knudsen and surface diffusivities, respectively
F = flow rate of effluent, LSTP/min
h = heat transfer coefficient between bed and wall, cal/cm^2·K·s
L = length of bed, cm
N = molar flux, mol/cm^2·s
P = total or partial pressure, MPa or psi
q = number of moles of sorbate adsorbed per gram of solid, mol/g solid
Q = heat of adsorption, cal/mol
r = radial distance from center of spherical particle, cm
R = gas constant
S = overall rate of sorption per unit volume of bed, mol/L·min
t = time, min or s
T = solid or bed temperature, K
u = superficial velocity, cm/min or cm/s
V_m = monolayer amount adsorbed, mol/g
x_i = mole fraction of species i in the adsorbed phase
y_i = mole fraction of species i in the gas phase
z = axial distance along the bed in feed direction, cm

Greek letters

α = interparticle void fraction
Δt = time step, min
ϵ = intraparticle void fraction
π = spreading pressure
ρ_B = bed density, g/cm^3
ρ_P = particle density, g/cm^3
θ = fractional surface coverage
τ = tortuosity
η = interaction parameter

Subscripts

A = CH_4
B = H_2
b = bed
g = gas
i = species, or cell or shell number
p = particle or purge
m = monolayer coverage
w = wall of the column

Superscripts

s = surface of particle
$-$ = volume-average quantity

Literature Cited

Basmadjian, D., and D. W. Wright, "Nonisothermal Sorption of Ethane-Carbon Dioxide Mixtures in Bed of 5A Zeolite," *Chem. Eng. Sci.*, **36,** 937 (1981).

Carter, J. W., and M. L. Wyszynski, "The Pressure Swing Adsorption Drying of Compressed Air," *Chem. Eng. Sci.*, **38,** 1,093 (1983).

Cassidy, R. T., and E. S. Holmes, "Twenty-five Years of Progress in Adiabatic Adsorption Processes," *AIChE Symp. Ser.*, **80**(233), 68 (1984).

Cen, P. L., and R. T. Yang, "Bulk Gas Separation by Pressure Swing Adsorption," *Ind. Eng. Chem. Fundam.*, (1986).

Chan, Y. N., F. B. Hill, and Y. H. Wong, "Equilibrium Theory of a Pressure Swing Adsorption Process," *Chem. Eng. Sci.*, **36,** 243 (1981).

Chen, W. N., and R. T. Yang, "Adsorption of Gas Mixtures and Modeling Cyclic Processes for Bulk, Multicomponent Gas Separation," in *Recent Developments in Separation Science,* N. N. Li and J. M. Calo, eds., CRC Press, Cleveland, **IX** (1985).

Cheng, H. C., and F. B. Hill, "Recovery and Purification of Light Gases by Pressure Swing Adsorption," in *Industrial Gas Separations, ACS Symp. Ser.* **223,** 195 (1983).

Chihara, K., and M. Suzuki, "Simulation of Nonisothermal Pressure Swing Adsorption," *J. Chem. Eng. Japan,* **16,** 53 (1983).

Costa, E., G. Galleja, and F. Domingo, "Adsorption of Gaseous Hydrocarbons on Activated Carbon," *AIChE J.*, **31**(6), 982 (1985).

Doong, S. J., and R. T. Yang, "A Comparison of Bulk Separation by Membrane and Pressure Swing Adsorption Processes," *Sep. Sc. Tech.*, (1986).

Fernandez, G. F., and C. N. Kenney, "Modeling of the Pressure Swing Air Separation Process," *Chem. Eng. Sci.*, **38,** 827 (1983).

Keller, G. E., "Gas-Adsorption Processes: State of the Art," in *Industrial Gas Separations,* T. E. Whyte, Jr., C. M. Yon, and E. H. Wagener, eds., Am. Chem. Soc., Washington, DC, 145 (1983).

Knaebel, K. S., "Analysis of Complementary Pressure Swing Adsorption," in *Fundamentals of Adsorption,* A. L. Myers, and G. Belfort, eds., 273–282, Engineering Foundation, New York (1984).

Liapis, A. I., and O. K. Crosser, "Comparison of Model Predictions with Nonisothermal Sorption Data for Ethane-CO_2 Mixtures in Beds of 5A Zeolite," *Chem. Eng. Sci.*, **37,** 958 (1982).

Liu, R. T., Calgon Corp. Private Communication (1984).

Myers, A. L., and J. M. Prausnitz, "Thermodynamics of Mixed Gas Adsorption," *AICHE J.*, **11,** 121 (1965).

Nakao, S., and M. Suzuki, "Effects of Preadsorption on Transient Processes in Cyclic Adsorption and Desorption," *J. Chem. Eng. Japan,* **16,** 330 (1983).

Nataraj, S., and P. C. Wankat, "Multicomponent Pressure Swing Adsorption," in *Recent Advances in Adsorption and Ion Exchange,* Y. H. Ma et al., eds., **78** AIChE, New York, (1982).

Ritter, J. A., "Adsorption of Multicomponent Gas Mixtures on Activated Carbon," M.S. Thesis, State Univ. New York, Buffalo (1985).

Ruthven, D. M., *Principles of Adsorption and Adsorption Processes,* Wiley, New York (1984).

Saunders, J. T., and R. T., Yang, "Equilibrium Adsorption of Gas Mixtures on Carbons," *Fuel,* **64,** 621 (1985).

Shendalman, L. H., and J. E. Mitchell, "A Study of Heatless Adsorption in the Model System CO_2 in He," *Chem. Eng. Sci.*, **27,** 1,449 (1972).

Sircar, S., "Separation of Multicomponent Gas Mixtures by Pressure Swing Adsorption," U.S. Patent 4,171,207 (1979).

Skarstrom, C. W., "Use of Adsorption Phenomenon in Automatic Plant-type Gas Analyzers," *Ann. NY Acad. Sci.*, **72,** 751 (1959).

Sladek, K. J., E. R., Gilliland and A. F., Baddour, "Diffusion on Surfaces. II: Correlation of Diffusivities of Adsorbed Species," *Ind. Eng. Chem. Fundam.*, **13,** 100 (1974).

Tsai, M. C., S. S. Wang, and R. T. Yang, "Pore Diffusion Model for Cyclic Separation," *AIChE J.*, **29,** 966 (1983).

Turnock, P. H., and R. H. Kadlec, "Separation of Nitrogen and Methane via Periodic Adsorption," *AIChE J.*, **17,** 335 (1971).

Wankat, P. C., and D. Tondeur, "Use of Multiple Sorbents in Pressure Swing Adsorption Parametric Pumping and Cycling Zone Adsorption," *AIChE Annual Meet.*, San Francisco, Paper 68d (1984).

Weaver, K., and C. E. Hamrin, Jr., "Separation of Hydrogen Isotopes by Heatless Adsorption," *Chem. Eng. Sci.*, **29,** 1,873 (1974).

Yagi, S, and N. Wakao, "Heat and Mass Transfer from Wall to Fluid in Packed Beds," *AIChE J.*, **5,** 79 (1959).

Yang, R. T., and P. L. Cen, "Improved Separation by Pressure Swing Adsorption by Using Inert Additives," *Ind. Eng. Chem. Proc. Des. Dev.*, (1986).

Yang, R. T., and S. J. Doong, "Gas Separation by Pressure Swing Adsorption: A Pore Diffusion Model for Bulk Separation," *AIChE J.*, **31,** 1,829 (1985).

Yang, R. T., J. B. Fenn, and G. L. Haller, "Modification to the Higashi Model for Surface Diffusion," *AIChE J.*, **19,** 1,052 (1973).

Yang, R. T., and R. T. Liu, "Gaseous Diffusion in Porous Solids at Elevated Temperatures," *Ind. Eng. Chem. Fundam.*, **21,** 262 (1982).

Yon, C. M., and P. H. Turnock, "Multicomponent Adsorption Equilibria on Molecular Sieves," *AIChE Symp. Ser.*, **67** (117), 3 (1971).

Manuscript received Feb. 26, 1985, and revision received May 21, 1985.